Time varying parameter models for catchments with land use change: the importance of model structure

S. Pathiraja[1,2], D.Anghileri[3], P. Burlando[3], A. Sharma[2] L. Marshall[2], H. Moradkhani[4]

[1]Institut für Mathematik

Universität Potsdam

Potsdam

GERMANY

Email: pathiraja@uni-potsdam.de

[2]Water Research Centre

School of Civil and Environmental Engineering

University of New South Wales

Sydney, NSW

AUSTRALIA

[3]Institute of Environmental Engineering

ETH Zurich

Zurich

SWITZERLAND

[4]Department of Civil, Construction and Environmental Engineering

University of Alabama

Tuscaloosa, Alabama

USA

Abstract

Rapid population and economic growth in South-East-Asia has been accompanied by extensive land use change with consequent impacts on catchment hydrology. Modelling methodologies capable of handling changing land use conditions are therefore becoming ever more important, and are receiving increasing attention from hydrologists. A recently developed Data Assimilation based framework that allows model parameters to vary through time in response to signals of change in observations is considered for a medium sized catchment (2880 km^2) in Northern Vietnam experiencing substantial but gradual land cover change. We investigate the efficacy of the method as well as the importance of the chosen model structure in ensuring the success of a time varying parameter method. The method was used with two lumped daily conceptual models (HBV and HyMOD) that gave good quality streamflow predictions during pre-change conditions. Although both time varying parameter models gave improved streamflow predictions under changed conditions compared to the time invariant parameter model, persistent biases for low flows were apparent in the HyMOD case. It was found that HyMOD was not suited to representing the modified baseflow conditions, resulting in extreme and unrealistic time varying parameter estimates. This work shows that the chosen model can be critical for ensuring the time varying parameter framework successfully models streamflow under changing land cover conditions. It can also be used to determine whether land cover changes (and not just meteorological factors) contribute to the observed hydrologic changes in retrospective studies where the lack of a paired control catchment precludes such an assessment.

1. Introduction

Population and economic growth in South-East Asia has led to significant land use change, with rapid deforestation occurring largely for agricultural purposes [*Kummer and Turner*, 1994]. Forest cover in the Greater Mekong Sub-region (comprising Myanmar, Thailand, Cambodia, Laos, Vietnam, and South China) has decreased from about 73% in 1973 to about 51% in 2009 [*WWF*, 2013]. Vietnam in particular has had the second highest rate of deforestation of primary forest in the world, based on estimates from the Forest Resource Assessment by the United Nations Food and Agriculture Organization [*FAO*, 2005]. Such extensive land use change has the potential to significantly alter catchment hydrology (in terms of both quantity and quality), with its effects sometimes not immediate but occurring gradually over a lengthy period of time. Recent estimates from satellite measurements indicate that rapid deforestation continues in the region, although at lower rates [e.g. *Kim et al.,* 2015]. Persistent land use change necessitates modelling methodologies that are capable of providing accurate hydrologic forecasts and predictions, despite non-stationarity in catchment processes. This is also particularly relevant for water resource management which requires reliable estimates of water availability, both in terms of volume and timing, to properly allocate the resource between different water uses and to prevent flood damages. Vietnam has built many reservoirs in the last decades and more are planned because they are considered to be fundamentally important for electricity production, flood control, water supply and irrigation, ultimately contributing to the development of the country [*Giuliani et al*., 2016].

The literature on land-use change and its impacts on catchment hydrology is extensive, with studies examining the effects of 1) conversion to agricultural land-use [*Thanapakpawin et al*, 2007; *Warburton et al.,* 2012]; 2) deforestation [*Costa et al.,* 2003; *Coe et al*, 2011]; 3) afforestation [e.g. *Yang et al., 2012*; *Brown et al*, 2013] and 4) urbanization [*Bhaduri et al.,* 2001; *Rose & Peters*, 2001]. Fewer studies have examined how traditional modelling approaches must be modified to handle

46 non-stationary conditions, or how modelling methods can be used to assess impacts of land use
47 change. Split sample calibration has been used frequently to retrospectively examine changes to
48 model parameters due to land use or climatic change [*Seibert & McDonnell, 2010; Coron et al., 2012;*
49 *McIntyre & Marshall*, 2010; *Legesse et al*, 2003]. Several other studies have employed scenario
50 modelling, whereby hydrologic models are parameterized to represent different possible future land
51 use conditions [e.g. *Niu & Sivakumar*, 2013; *Elfert & Borman*, 2010]. A related approach involves
52 combining land use change forecast models with hydrologic models [e.g. *Wijesekara et al.,* 2012].
53 However, the aforementioned approaches are unsuited to hydrologic forecasting in changing
54 catchments, as the predicted land use change may not reflect actual changes. A potentially more
55 suitable approach in such a setting is to allow model parameters to vary in time, rather than
56 assuming a constant optimal value or stationary probability distribution. Many existing methods
57 utilising such a framework require some *apriori* knowledge of the land use change in order to inform
58 variations in model parameters (see for instance *Efstratiadis,* 2015; *Brown et al.,* 2006; and *Westra et*
59 *al.,* 2014). Recent efforts have examined the potential for time varying parameter models to
60 automatically adapt to changing conditions using information contained in hydrologic observations
61 and sequential Data Assimilation, without requiring explicit knowledge of the changes [see for
62 example *Taver et al.,* 2015, *Pathiraja et al.,* 2016a&b]. Such approaches can objectively modify
63 model parameters in response to signals of change in observations in real time, whilst simultaneously
64 providing uncertainty estimates of parameters and streamflow predictions. They can also be used to
65 determine whether land cover changes (and not solely meteorological factors) contribute to
66 observed changes in streamflow dynamics in retrospective studies where the lack of a paired control
67 catchment precludes such an assessment.
68
69 *Pathiraja et al.* [2016a] presented an Ensemble Kalman Filter based algorithm (the so-called Locally
70 Linear Dual EnKF) to estimate time variations in model parameters. The method sequentially
71 assimilates observations into a numerical model in real time to generate improved estimates of

72 model states, fluxes and parameters based on their respective uncertainties. Its purpose is to infer
73 changes to catchment properties (e.g. land cover change) from hydrologic observations, without
74 prior knowledge of such changes, at the time scale of the available observations. It can therefore be
75 used for various applications: 1) to retrospectively estimate time variations in model parameters; 2)
76 for short-term predictive modelling (days to weeks), e.g. flood forecasting; and 3) for on-line/real
77 time water resource management, e.g. determining releases from reservoirs in catchments with
78 changing land cover conditions. In retrospective mode, the method is advantageous compared to
79 split-sample calibration type approaches since no *apriori* knowledge of land use change is needed,
80 and the modeller does not have to make somewhat arbitrary decisions about how to segregate the
81 data. When used for prediction or forecasting, states and parameters are updated sequentially using
82 all available observations up until the current time. These updated states and parameters are then
83 used along with the prior parameter generating model to produce hydrologic predictions over a short
84 time horizon. This allows one to seamlessly obtain predictions without the modeller needing to
85 explicitly modify the model to account for any catchment changes. The efficacy of the method was
86 demonstrated in *Pathiraja et al.* [2016b] through an application to small experimental catchments (<
87 350 ha) with drastic land cover changes and strong signals of change in streamflow observations.
88
89 Here we investigate two issues related to the use of time varying parameter models for prediction in
90 realistic catchments with changing land cover conditions. Firstly, we investigate the efficacy of the
91 time varying parameter method for sparsely observed, medium-sized catchments with spatially
92 complex and gradual land use change (occurring over months/years). Several authors have
93 demonstrated that impacts of land use change on the hydrologic response are dependent on many
94 factors including the type and rate of land cover conversion as well the spatial pattern of different
95 land uses within the catchment [*Dwarakish & Ganasri*, 2015; *Warburton et al.*, 2012]. In such
96 situations, the effects of unresolved spatial heterogeneities in model inputs (e.g. rainfall) and the
97 relatively less pronounced changes in land surface conditions make time varying parameter detection

98 and accurate hydrologic prediction more difficult. The second objective is to examine the role of
99 the hydrologic model in determining the ability of the time varying parameter framework to provide
100 high quality predictions in changing conditions. Often there may be several candidate hydrologic
101 models (with time invariant parameters) that have similar predictive performance for a catchment
102 when calibrated and validated over a time series of static land cover conditions [*Marshall et al.,*
103 2006]. This work examines whether all such candidate models in time varying parameter mode are
104 also capable of providing accurate predictions under changing conditions.
105
106 These issues are investigated for the Nammuc catchment (2880 km^2) in Northern Vietnam which has
107 experienced deforestation largely due to increasing agricultural development. It serves as an ideal
108 test catchment to study the efficacy of the time varying parameter algorithm due to its size, spatially
109 complex pattern of land use changes, and lack of information on the precise timing of such changes.
110 Land cover change is estimated to have occurred at varying rates, with cropland accounting for
111 roughly 23% between 1981 and 1994, and 52% by 2000. We also consider two lumped conceptual
112 hydrologic models (given the availability of point rainfall, temperature, and streamflow data)
113 operating at daily time step to address the second objective. Both models demonstrate similar
114 performance in representing streamflow at the outlet during the pre-change calibration period
115 (1975-1979), although their performance during/after land use change is unknown. Therefore, the
116 effect of the model structure (i.e. model equations) on hydrologic predictions from the time varying
117 parameter models is studied. This work represents the first application of a continuously time
118 varying parameter approach for modelling a real medium sized catchment with no *apriori* (or partial)
119 knowledge of the type and timing of land use change.
120
121 The remainder of this paper is structured as follows. Details of the study catchment and the impact
122 of land cover change are analysed in Section 2. Section 3 summarizes the experimental setup
123 including the hydrological models and the time varying parameter estimation method used. Results

are provided in Section 4, along with an analysis of whether the time varying model structures reflect the observed catchment dynamics. Finally, we conclude with a summary of the main outcomes of the study as well as proposed future work.

2. The Nammuc Catchment

The Nammuc catchment (2880 km^2) is located in the Red River Basin, the second largest drainage basin in Vietnam which also drains parts of China and Laos. The local climate is tropical monsoon dominated with distinct wet (May to October) and dry (November to April) seasons. The wet season tends to have high temperatures (on average 27 to 29 °C) due to south-south easterly winds that bring humid air masses. Conversely, during the dry season, circulation patterns reverse carrying cooler dry air masses to the basin (leading to average temperatures of 16 to 21°C). Streamflow response is consequently monsoon driven, with high flows occurring between June and October (generally peaking in July/August) and low flows in the December to May period (Vu, 1993). Average annual rainfall at Nammuc varies between 1300 and 2000 mm (on average 1600 mm) and catchment elevation ranges between 350 and 1500 m asl. A summary of catchment properties is provided in Table 1 for pre-change (prior to 1994) and post-change (after 1994) conditions. This separation was based on available land cover information as described below.

2.1.Data & Land Cover Change

Figure 1 shows the available land cover information for the Nammuc catchment. Land cover information for the catchment is scant, we were able to locate only two sources which unfortunately do not give a complete picture over the entire time period of interest (1970 to 2004). The first land cover map refers to the period 1981-1994 and was obtained by the Vietnamese Forest Inventory and Planning Institute (http://fipi.vn/Home-en.htm). The second land cover map refers to year 2000 and was obtained from the FAO Global Land Cover database (http://www.fao.org/geonetwork/srv/en/metadata.show?id=12749&currTab=simple). A comparison

148 of the two maps shows a reduction in forest cover in favor of cropland; Evergreen Leaf decreases
149 from about 60% to 30% whilst cropland increases from about 23% to 52%. The change in land cover
150 is patchy, although mostly concentrated in the northern part of the catchment. Because of the scant
151 information available, it is not easy to identify the precise time period of these changes. Based on the
152 available land cover map information and the changes to observed runoff (see Section 2.2), we posit
153 that a period of rapid extensive deforestation occurred in early to mid-1990s.
154
155 Daily point rainfall data is available at four precipitation stations surrounding the catchment (Dien
156 Bien, Tuan Giao, Quynh Nhai and Nammuc, see Figure 1). Catchment averaged rainfall was
157 developed as a weighted sum of the four stations with weights determined by Thiessen Polygons.
158 Daily mean temperature was calculated in a similar fashion using temperature records from the 2
159 closest gauges (Lai Chau and Quynh Nhai, see Figure 1). This was used to estimate Potential
160 Evapotranspiration through the empirical temperature-latitude based Hamon PET method [*Hamon*,
161 1961]. Daily rainfall, temperature and streamflow data was provided by the Vietnamese Institute of
162 Water Resources Planning.

163 2.2.Impact of Land Cover Change on Streamflow

164 The annual runoff/direct runoff coefficient and Baseflow Index were used to assess the impact of
165 land cover change on the hydrologic regime. Baseflow was estimated using the two parameter
166 recursive baseflow filter of *Eckhardt* [2005] (see equation 1), with on-line updating of baseflow
167 estimates to match low flows:

$$b_k = \frac{1}{(1 - a.BFI_{max})}[(1 - BFI_{max}).a.b_{k-1} + (1 - a).BFI_{max}.y_k] \quad (1)$$

168 where b_k is the estimated baseflow at time k, y_k is the total observed streamflow at time k, BFI_{max}
169 is the maximum value of the BFI (long term ratio of baseflow to total streamflow) and a is a filter
170 parameter. In this study, we adopt $BFI_{max} = 0.5$ and $a = 0.988$ based on manual optimization.
171

An examination of the observed streamflow and rainfall records shows that distinct changes to the hydrologic regime are evident after the mid-1990s. The annual runoff coefficient $\left(\frac{runoff}{rainfall}\right)$ varies between 0.4 and 0.6 prior to 1994, after which it increases to between 0.6 and 0.8 until 2004 (see Figure 2a). However, increases to annual yields are driven mostly by changes to baseflow volume. This is evident in Figure 2a, which shows that the increase in the annual direct runoff coefficient $\left(\frac{runoff-baseflow}{rainfall}\right)$ is less than the increase in the total runoff coefficient (roughly 0.1 increase compared to 0.2 respectively). A small increase in the Annual Baseflow Index $\left(\frac{baseflow}{runoff}\right)$ is apparent also, from about 0.32 on average in the period 1970 to 1982 to 0.39 on average after 1994 (Figure 2b). This indicates that the annual increases to baseflow volume exceed the increases to direct runoff volume. Similar changes were found by *Wang et al.* [2012] who analyzed records in the entire Da River basin which drains the largest river in the Red River catchment. The exact physical processes behind the observed increase in baseflow are not precisely known, particularly since effects of land use change from forest to cropland are not unequivocal [*Price*, 2011]. Deforestation may be associated to an increase in mean annual flow and baseflow because of lower interception and evapotranspiration rates [e.g., *Keppeler and Ziemer*, 1990]. Nevertheless, permanent forest removal may decrease baseflow because of soil compaction and lower infiltration rates [e.g., *Zimmermann et al.,* 2006; *Bormann and Klaassen;* 2008]. Some authors also show that tillage practices, associated to forest conversion to cropland, can increase soil porosity, soil water content, and infiltration, thus ultimately contributing to baseflow formation [e.g., *Alam et al.,* 2014].

At a seasonal time scale, it is apparent that both wet and dry season flows exhibit temporal variations. We utilized the Moving Average Shifting Horizon (MASH) [*Anghileri et al.,* 2014] and Mann-Kendall test to assess seasonal trends in observed streamflow, precipitation, and temperature data. The MASH tool can be used to qualitatively assess inter-annual variations in the seasonal pattern of a variable. It works by calculating a statistic of the data (e.g. mean) over the same block of

197 days in consecutive years. A steady increase in baseflow is again apparent (see February to April in
198 Figure 2c), as well as increases to wet season flows (see June to September in Figure 2c). Mann-
199 Kendall test (with significance level equal to 5%) on annual and monthly streamflow time series
200 shows increasing trends in almost all months, i.e., from October to July. No concurrent increases are
201 apparent in rainfall (see Figure 2d). Also, the Mann-Kendall test applied to precipitation time series
202 does not show any statistically significant trend, except a decrease in September for Nammuc and
203 Quynh Nhai station and an increase in July for Dien Bien station. Temperature variations are not
204 evident from the MASH analysis (not shown) and no significant trend can be detected by applying the
205 Mann-Kendall test. These results indicate that changes in streamflow dynamics are likely due to land
206 use change rather than climatic impacts.

207 # 3. Experimental Setup

208 ## 3.1.Hydrologic Models

209 Conceptual lumped models operating at a daily time step were adopted due to the availability of
210 point rather than distributed hydro-meteorological data of sufficient length. We considered the
211 HyMOD [*Boyle*, 2001] and Hydrologiska Byrans Vattenbalansavdelning (HBV) [*Bergstrom et al.,* 1995]
212 models. They differ mainly in the way components of the response flow are separated (HBV has near
213 surface flow, interflow, and baseflow components whilst HyMOD has a quickflow and slow flow
214 component only) and how these flows are routed. A schematic of the models is shown in Figure 3.
215
216 In the HyMOD model, spatial variations in catchment soil storage capacity are represented by a
217 Pareto distribution with shape parameter b and maximum point soil storage depth c_{max}. Excess
218 rainfall (V) is partitioned into three cascading tanks representing quick flow and a single slow flow
219 store through the splitting parameter α. Outflow from these linear routing tanks is controlled by

220 parameters k_q (for the quick flow stores) and k_s (for the slow flow store). The model has a total of 5
221 states and 5 parameters.
222
223 In the HBV model, input to the soil store is represented by a power-law function (see Figure 3, note
224 the snow store is neglected for this study). Excess rainfall enters a shallow layer store which
225 generates: 1) near surface flow (q_0) whenever the shallow store state ($stw1$) is above a threshold
226 ($hl1$) and 2) interflow (q_1) by a linear routing mechanism controlled by the $K1$ parameter.
227 Percolation from the shallow layer store to the deep layer store (controlled by $perc$ parameter) then
228 leads to the generation of baseflow also via linear routing (controlled by the $K2$ parameter). Finally, a
229 triangular weighting function of base length $Maxbas$ is used to route the sum of all three flow
230 components. There are a total of 9 parameters and 3 states.
231
232 The Shuffled Complex Evolution Algorithm (SCE-UA) [*Duan et al.*, 1993] was used to calibrate HyMOD
233 and the Borg Evolutionary Algorithm [*Hadka & Reed*, 2013] was used to calibrate HBV. The
234 calibration algorithms were selected based on previous studies that had successfully used them for
235 calibration of these models [*Reed et al.,* 2013; *Moradkhani et al.,* 2005]. The calibration procedure
236 itself is however not critical in our study, because the optimal parameter values are only used as
237 initial values for the time varying parameter method. Both models were calibrated to pre-change
238 conditions. The period 1973 to 1979 was selected for calibration (with 2 years for spin-up) as it was
239 expected to have minimal land cover changes (and is therefore representative of pre-change
240 conditions), and also to ensure sufficient data on pre-change conditions is available for assimilation.
241 Both models had very similar performance in terms of reproducing observed runoff (an NSE of 0.75
242 and 0.77 for HyMOD and HBV respectively). HBV was slightly better at reproducing low flows whilst
243 HyMOD was slightly better at mid-range flows (see Table 2). Here the low flow threshold was
244 defined as the average annual 50th percentile flow and the high flow threshold as the average annual
245 85th percentile flow.

3.2.Time Varying Parameter Estimation

A Data Assimilation based framework for estimating time varying parameters was presented in *Pathiraja et al.* [2016a]. The approach relies on an Ensemble Kalman Filter (EnKF) [*Evensen*,1994] to perform sequential joint state and parameter updating. EnKFs were developed to extend the applicability of the celebrated Kalman Filter [*Kalman,* 1960] to non-linear systems, although they provide a sub-optimal update as only the mean and covariance are considered in generating the posterior. However, they have been used with much success in many hydrologic applications [see for example *Reichle et al.,* 2002; *Gu et al.*, 2005; *Komma et al.,* 2008; *Sun et al.,* 2009; *Xu et al.,* 2016]. EnKFs offer a practical alternative to Sequential Monte Carlo/Particle Filter methods that propagate the full probability density through time, but suffer from several implementation issues even in moderate dimensional systems. The Locally Linear Dual EnKF method of *Pathiraja et al.* [2016a] works by sequentially proposing parameters, updating these using the Ensemble Kalman filter and available observations, and subsequently using these updated parameters to propose and update model states. An approach for proposing parameters in the time varying setting was also presented, for cases where no prior knowledge of parameter variations is available. The method was verified against multiple synthetic case studies as well as for 2 small experimental catchments experiencing controlled land use change [*Pathiraja et al.,* 2016a and *Pathiraja et al.,* 2016b]. The algorithm is summarised below, for full details refer to *Pathiraja et al.* [2016a].

3.2.1. Locally Linear Dual EnKF

Suppose a dynamical system can be described by a vector of states $\boldsymbol{x}_t$ and outputs $\boldsymbol{y}_t$ and a vector of associated model parameters $\boldsymbol{\theta}_t$ at any given time *t.* The uncertain system states and parameters are represented by an ensemble of states $\{\boldsymbol{x}_t^i\}_{i=1:n}$ and parameters $\{\boldsymbol{\theta}_t^i\}_{i=1:n}$ each with *n* members. The prior state and parameter distributions $\{\boldsymbol{x}_t^{i-}\}_{i=1:n}$ and $\{\boldsymbol{\theta}_t^{i-}\}_{i=1:n}$ respectively represent our prior knowledge of the system, usually derived as the output from a numerical model. Suppose also that the system outputs are observed $(\boldsymbol{y}_t^o)$ but that there is also some uncertainty associated with

these observations. The purpose of the data assimilation algorithm (here the EnKF) is to combine the prior estimates with measurements, based on their respective uncertainties, to obtain an improved estimate of the system states and parameters. A single cycle of the Locally Linear Dual EnKF procedure for a given time *t* is undertaken as follows. Note in the following, the overbar notation is used to indicate the ensemble mean.

1. ***Propose a prior parameter ensemble.*** This involves generating a parameter ensemble using prior knowledge. In this case, our prior knowledge comes from the updated parameter ensemble from the previous time ($\boldsymbol{\theta}_{t-1}^{i+}$) and how it has changed over recent time steps. The assumed parameter dynamics is a Gaussian random walk with time varying mean and variance, given by:

$$\boldsymbol{\theta}_t^{i-} \sim N\left(\boldsymbol{\theta}_{t-1}^{i+} + \boldsymbol{m}_t.\Delta t\,, s^2\boldsymbol{\Sigma}_{t-1}^{\theta}\right) \; for\; i = 1{:}n \tag{2}$$

$$\boldsymbol{\Sigma}_{t-1}^{\theta} = \frac{1}{n-1}\sum_{i=1}^{n}\left(\boldsymbol{\theta}_{t-1}^{i+} - \overline{\boldsymbol{\theta}_{t-1}^{+}}\right)\left(\boldsymbol{\theta}_{t-1}^{i+} - \overline{\boldsymbol{\theta}_{t-1}^{+}}\right)^{\mathrm{T}} \tag{3}$$

where $\boldsymbol{\Sigma}_{t-1}^{\theta}$ is the sample covariance matrix of the updated parameter ensemble at time $t-1$; $\overline{\boldsymbol{\theta}_{t-1}^{+}}$ indicates the ensemble mean of the updated parameters at time $t-1$; $(\,)^{\mathrm{T}}$ represents the transpose operator; and s^2 is a tuning parameter. The prior ensemble mean is determined as the linear extrapolation of the updated ensemble means from the previous two time steps, i.e.:

$$\boldsymbol{m}_t[k] = \begin{cases} \boldsymbol{m}_{t-1}[k], & |\boldsymbol{m}_{t-1}[k]| \le m_{max} \\ \boldsymbol{m}_{t-2}[k], & |\boldsymbol{m}_{t-1}[k]| > m_{max} \end{cases} \tag{4}$$

$$\boldsymbol{m}_{t-1} = \frac{\overline{\boldsymbol{\theta}_{t-1}^{+}} - \overline{\boldsymbol{\theta}_{t-2}^{+}}}{\Delta t} \tag{5}$$

$$\boldsymbol{m}_{t-2} = \frac{\overline{\boldsymbol{\theta}_{t-2}^{+}} - \overline{\boldsymbol{\theta}_{t-3}^{+}}}{\Delta t} \tag{6}$$

where $\boldsymbol{m}_t[k]$ indicates the kth component of the vector $\boldsymbol{m}_t$, the estimated rate of change. Note that the extrapolation is forced to be less than a pre-defined maximum rate of change m_{max} to minimise overfitting and avoid parameter drift due to isolated large updates. The

maximum rate of change is model specific and will depend on the modeller's judgement regarding expected extreme changes.

2. ***Consider observation and forcing uncertainty.*** This is done by perturbing measurements of forcings and system outputs with random noise sampled from a distribution representing the uncertainty in those measurements. The result is an ensemble of forcings ($\boldsymbol{u}_t^i$) and observations ($\boldsymbol{y}_t^i$) each with *n* members. For example, if random errors in measurements of system outputs (herein also referred as observations) are characterized by a zero mean Gaussian distribution, the ensemble of observations is given by:

$$\boldsymbol{y}_t^i \sim N\left(\boldsymbol{y}_t^o, \boldsymbol{\Sigma}_t^{y^o y^o}\right) \; for\; i = 1{:}n \tag{7}$$

where $\boldsymbol{y}_t^o$ is the recorded measurement at time t and $\boldsymbol{\Sigma}_t^{y^o y^o}$ is the error covariance matrix of the measurements.

3. ***Generate simulations using prior parameters***. The prior parameters from Step 1, $\boldsymbol{\theta}_t^{i-}$ and updated states from the previous time, $\boldsymbol{x}_{t-1}^{i+}$ are forced through the model equations to generate an ensemble of model simulations of states ($\widehat{\boldsymbol{x}}_t^i$) and outputs ($\widehat{\boldsymbol{y}}_t^i$):

$$\widehat{\boldsymbol{x}}_t^i = f\left(\boldsymbol{x}_{t-1}^{i+}, \boldsymbol{\theta}_t^{i-}, \boldsymbol{u}_t^i\right) \; for\; i = 1{:}n \tag{8}$$

$$\widehat{\boldsymbol{y}}_t^i = h\left(\widehat{\boldsymbol{x}}_t^i, \boldsymbol{\theta}_t^{i-}\right) \; for\; i = 1{:}n \tag{9}$$

4. ***Perform the Kalman update of parameters.*** Parameters are updated using the Kalman update equation and the prior parameter and simulated output ensemble from Step 1 and 3:

$$\boldsymbol{\theta}_t^{i+} = \boldsymbol{\theta}_t^{i-} + \mathbf{K}_t^{\theta}\left(\boldsymbol{y}_t^i - \widehat{\boldsymbol{y}}_t^i\right) \; for\; i = 1{:}n \tag{10}$$

$$\mathbf{K}_t^{\theta} = \boldsymbol{\Sigma}_t^{\theta\hat{y}}\left[\boldsymbol{\Sigma}_t^{\hat{y}\hat{y}} + \boldsymbol{\Sigma}_t^{y^o y^o}\right]^{-1} \tag{11}$$

where $\boldsymbol{\Sigma}_t^{\theta\hat{y}}$ is a matrix of the sample cross covariance between errors in parameters $\boldsymbol{\theta}_t^{i-}$ and simulated output $\widehat{\boldsymbol{y}}_t^i$; and $\boldsymbol{\Sigma}_t^{\hat{y}\hat{y}}$ is the sample error covariance matrix of the simulated output:

$$\boldsymbol{\Sigma}_t^{\theta\hat{y}} = \frac{1}{n-1}\sum_{i=1}^{n}\left(\boldsymbol{\theta}_t^{i-} - \overline{\boldsymbol{\theta}_t^{-}}\right)\left(\widehat{\boldsymbol{y}}_t^i - \overline{\widehat{\boldsymbol{y}}_t}\right)^{\mathrm{T}} \tag{12}$$

$$\boldsymbol{\Sigma}_t^{\hat{y}\hat{y}} = \frac{1}{n-1}\sum_{i=1}^{n}\left(\widehat{\boldsymbol{y}}_t^i - \overline{\widehat{\boldsymbol{y}}_t}\right)\left(\widehat{\boldsymbol{y}}_t^i - \overline{\widehat{\boldsymbol{y}}_t}\right)^{\mathrm{T}} \tag{13}$$

5. ***Generate simulations using updated parameters.*** Step 3 is repeated with the updated parameter ensemble $\boldsymbol{\theta}_t^{i+}$ to generate the prior ensemble of model simulations of states ($\boldsymbol{x}_t^{i-}$) and outputs ($\widetilde{\boldsymbol{y}}_t^i$):

$$\boldsymbol{x}_t^{i-} = f\left(\boldsymbol{x}_{t-1}^{i+}, \boldsymbol{\theta}_t^{i+}, \boldsymbol{u}_t^i\right) \; for\, i = 1{:}\, n \tag{14}$$

$$\widetilde{\boldsymbol{y}}_t^i = h\left(\boldsymbol{x}_t^{i-}, \boldsymbol{\theta}_t^{i+}\right) \; for\, i = 1{:}\, n \tag{15}$$

6. ***Perform the Kalman update of states and outputs***. Use the Kalman update equation for correlated measurement and process noise (equations 16 to 19) and the simulated state ($\boldsymbol{x}_t^{i-}$) and output ($\widetilde{\boldsymbol{y}}_t^i$) ensembles from Step 5 to update them. Since the measurements have already been used to generate $\widetilde{\boldsymbol{y}}_t^i$, the errors in model simulations and measurements are now correlated. The standard Kalman update equation (as in the form of equations 10 and 11) can no longer be used as it relies on the assumption that errors in measurements and model simulations are independent.

$$\boldsymbol{x}_t^{i+} = \boldsymbol{x}_t^{i-} + \mathbf{K}_t^x\left(\boldsymbol{y}_t^i - \widetilde{\boldsymbol{y}}_t^i\right) \; for\, i = 1{:}\, n \tag{16}$$

$$\mathbf{K}_t^x = \left[\boldsymbol{\Sigma}_t^{x\tilde{y}} + \boldsymbol{\Sigma}_t^{\varepsilon_x y^o}\right]\left[\boldsymbol{\Sigma}_t^{\tilde{y}\tilde{y}} + \boldsymbol{\Sigma}_t^{\varepsilon_{\tilde{y}} y^o} + \left(\boldsymbol{\Sigma}_t^{\varepsilon_{\tilde{y}} y^o}\right)^{\mathrm{T}} + \boldsymbol{\Sigma}_t^{y^o y^o}\right]^{-1} \tag{17}$$

$$\boldsymbol{\varepsilon}_{x_t}{}^i = \boldsymbol{x}_t^{i-} - \widehat{\boldsymbol{x}}_t^i \tag{18}$$

$$\boldsymbol{\varepsilon}_{\tilde{y}_t}{}^i = \widetilde{\boldsymbol{y}}_t^i - \widehat{\boldsymbol{y}}_t^i \tag{19}$$

where $\boldsymbol{\Sigma}_t^{x\tilde{y}}$ is a matrix of the sample cross covariance between simulated states $\left\{\boldsymbol{x}_t^{i-}\right\}_{i=1:n}$ and outputs $\left\{\widetilde{\boldsymbol{y}}_t^i\right\}_{i=1:n}$ from Step 5; $\boldsymbol{\Sigma}_t^{\varepsilon_x y^o}$ represents the sample covariance between $\left\{\boldsymbol{\varepsilon}_{x_t}{}^i\right\}_{i=1:n}$ and the observations; and $\boldsymbol{\Sigma}_t^{\varepsilon_{\tilde{y}} y^o}$ represents the sample covariance between the $\left\{\boldsymbol{\varepsilon}_{\tilde{y}_t}{}^i\right\}_{i=1:n}$ and the observations.

The above algorithm specifies the updating of states and parameters at any given time, based on available observations. This allows one to retrospectively estimate time variations in model parameters, as well as provide one time step ahead forecasts of states & outputs (as per equations 8 and 9). Forecasts at longer time horizons (i.e. longer than one time step ahead) would be made by

generating prior parameters and states as detailed in Steps 1 to 3, although the local linear extrapolations are only valid close to the current time point.

3.2.2. Application to the Nammuc Catchment

Joint state and parameter estimation was undertaken for the Nammuc Catchment over the period 1979 to 2004 by assimilating streamflow observations into the HyMOD and HBV models at a daily time step. Estimating a large number of parameters from limited data is problematic in that the system is highly under-determined, making it difficult to ensure the estimated parameters are meaningful. Given the fairly low parameter dimensionality of HyMOD, all model parameters were allowed to vary in time whilst for HBV we applied the Sobol method to identify the most sensitive parameters to be included in the time varying parameter estimation. The Sobol method is a global sensitivity analysis method based on variance decomposition. It identifies the partial variance contribution of each parameter to the total variance of the hydrological model output [see for example *Saltelli et al.,* 2008, *Nossent et al. 2011*]. The method, implemented through the SAFE toolbox [*Pianosi et al.,* 2015], found the lp and $Maxbas$ parameters to be the least sensitive and least important in defining variations to catchment hydrology (see Table 3). These were held fixed (lp = 1 and $Maxbas$ = 1 day) in the following analysis. Note that although the $hl1$ parameter was found to have low sensitivity, it was retained as a time varying parameter due to its conceptual importance in separating interflow and near surface flow (refer Figure 3).

Unbiased normally distributed ensembles of the parameters and states are required to initialise the LL Dual EnKF. Initial parameter ensembles were generated by sampling from a Gaussian distribution with mean equal to the calibrated parameters over the pre-change period and variance estimated from parameter sets with similar objective function values. Parameter sets with similar objective function values were obtained when using different starting points to the optimization algorithm during the model calibration stage. Initial state ensembles were also sampled from normal

distributions with mean equal to the simulated state at the end of the calibration period. An ensemble size of 100 members was adopted and assumed sufficiently large based on the findings of *Moradkhani et al.* [2005] and *Aksoy et al.* [2006]. Due to the stochastic-dynamic nature of the method, ensemble statistics were calculated over 20 separate realisations of the LL Dual EnKF. The prior parameter generating method described in Step 1 of Section 3.2 requires specification of the tuning parameter s^2 to define the variance of the perturbations. This was tuned by selecting the s^2 value that optimized the quality of forecast streamflow over the calibration period. Forecast quality was assessed using the logarithmic score (LS) [*Good,* 1952] of background streamflow predictions ($\tilde{y}_t^i$) using updated parameters (equation 15), which was averaged over the calibration period of length *T*:

$$\overline{LS} = \sum_{t=1}^{T} LS_t \quad (20)$$

$$LS_t = \log\left(f(y = y_t^o)\right) \quad (21)$$

where $f(y)$ is the probability density function of the background streamflow predictions (represented by the empirical pdf of the sample points $\{\tilde{y}_t^i\}_{i=1:n}$); and y_t^o is the measurement of the system outputs. The s^2 value that gave the largest $\overline{LS}$ was adopted for the assimilation period. The maximum allowable daily rate of change in the ensemble mean was based on assuming a linear rate of change within the entire feasible parameter space over a three year period.

As detailed in Section 3.2, observation and forcing uncertainty is considered by perturbing measurements with random noise. Here streamflow errors were assumed to be zero-mean normally distributed (truncated to ensure positivity) and heteroscedastic. The variance is defined as a proportion of the observed streamflow, to reflect the fact that larger flows tend to have greater errors than low flows:

$$y_t^i \sim TN(y_t^o, d.y_t^o) \ \ for\ i = 1{:}n \quad (22)$$

where TN indicates the truncated normal distribution to ensure positive flows and d = 0.1. A multiplier of 0.1 was chosen based on estimates adopted for similar gauges in hydrologic DA studies [e.g. *Clark et al.,* 2008; *Weerts & Serafy,* 2006; *Xie et al.,* 2014].

Several studies have noted that a major source of rainfall uncertainty arises from scaling point rainfall to the catchment scale [*Villarini & Krajewski*, 2008; *McMillan et al.*, 2011] and that multiplicative errors models are suited to describing such errors [e.g. *Kavetski et al.*, 2006]. Rainfall uncertainties were therefore described using unbiased, lognormally distributed multipliers:

$$P_t^i = P_t . M^i \quad (23)$$

$$M^i \sim LN(m, v) \text{ and } X^i = \log\left(M^i\right) \sim N(\mu, \sigma^2) \quad for\ i = 1{:}n \quad (24)$$

where P_t is the measured rainfall at time t; m and v are the mean and variance of the lognormally distributed rainfall multipliers M respectively; and μ and σ^2 are the mean and variance of the normally distributed logarithm of the rainfall multipliers M. For unbiased perturbations, we let m = 1. The variance of the rainfall multipliers (v) was estimated by considering upper and lower bound error estimates in the Thiessen weights assigned to the four rainfall stations (see Section 2.1 for calculation of catchment averaged rainfall, P_t). The resulting upper and lower bound catchment averaged rainfall data were then used to estimate error parameters due to spatial variation in rainfall:

$$v = e^{(2\mu + \sigma^2)} . \left(e^{\sigma^2} - 1\right) \quad (25)$$

$$\sigma^2 = \widehat{\sigma^2} = var\left(\log\left[\frac{P_{upper,10}}{P_{lower,10}}\right]\right) \quad (26)$$

$$\mu = \log(m) - \frac{\sigma^2}{2} = -\frac{\sigma^2}{2} \quad (27)$$

where $P_{upper,10}$ indicates catchment averaged rainfall data estimated using the upper bound Thiessen weights with daily depth greater than 10mm (similar for $P_{lower,10}$). A 10mm rainfall depth threshold was chosen to avoid large rainfall fractions due to small rainfall depths. $\widehat{\sigma^2}$ was found to be 0.05 in this case study. Similarly, we assume the dominant source of uncertainty in temperature

data arises from spatial variation. Differences in temperature records at Lai Chau and Quynh Nhai (only available gauges with temperature records) were analysed and found to be approximately normally distributed with sample mean 0.2 deg C and variance of 1.4 deg C. A perturbed temperature ensemble was then generated according to equation 28:

$$T_t^i \sim TN\left(T_t^{avg}, 1.4\right) \quad for \ i = 1{:}n \tag{28}$$

where T_t^{avg} represents catchment averaged temperature data (see Section 2.1). Note that perturbations were taken to be unbiased (zero mean) as the sample mean of the differences in the temperature records was close to zero. The same perturbed input and observation sequences were used for the HyMOD and HBV runs for the sake of comparison. A summary of the values adopted for the various components of the Locally Linear Dual EnKF for each model is provided in Table 4 and Table 5.

4. Results and Discussion

Temporal variations in the estimated parameter distributions from the LL Dual EnKF are evident for both models (see Figure 4 and 5). In the case of the HBV model, changes at an inter-annual time scale are evident for the $perc$ and β (see Figure 4). The decrease in the β parameter means that a greater proportion of rainfall is converted to runoff (i.e. more water entering the shallow layer storage). Additionally, the increase in the $perc$ parameter means that a greater volume of water is made available for baseflow generation. These changes correspond with the observed increase in the annual runoff coefficient (Figure 2) and increase in baseflow volume (as discussed in Section 2.2). From an algorithm perspective, these parameters are most strongly correlated with streamflow (as well as the most sensitive, see Table 3), meaning that they will receive the greatest proportional updates. Similar parameter adjustments are seen for HyMOD, at least at a qualitative level (see Figure 5). The sharp increase in the b parameter during the post-change period means that a greater volume of water is available for routing (as larger b values mean that a smaller proportion of the

414 catchment has deep soil storage capacity) and the downward inter-annual trend in α means that a
415 greater portion of excess runoff is routed through the baseflow store. Intra-annual variations in
416 updated model parameters for both HyMOD and HBV are also apparent (refer Figure 4 and Figure 5).
417 This is due to the inability of a single parameter distribution to accurately model both wet and dry
418 season flows. Such variations were not observed when using the time varying parameter framework
419 for small deforested catchments (< 350ha) [see *Pathiraja et al.,* 2016b]. The comparatively less clear
420 parameter changes for the Nammuc catchment are due to a combination of the increased difficulty
421 in accurately modelling the hydrologic response (even in pre-change conditions) and due to the
422 relatively more subtle and gradual changes to land cover. Nonetheless, the method is shown to
423 generate a temporally varying structure that is conceptually representative of the observed changes.
424
425 Despite the overall correspondence between changes to model parameters and observed
426 streamflow, a closer examination shows that the hydrologic model structure is critical in determining
427 whether the time varying parameter models accurately reflect changes in all aspects of the
428 hydrologic response (not just total streamflow). In order to examine the impact of parameter
429 variations on the model dynamics, we generated model simulations with the time varying parameter
430 ensemble from the LL Dual EnKF, but without state updating (hereafter referred to as TVP-HBV and
431 TVP-HyMOD). Streamflow predictions from the LL Dual EnKF (i.e. with state and parameter updating)
432 for both the HyMOD and HBV are generally of similar quality and superior to those from the
433 respective time invariant parameter models, although a slight bias in baseflow predictions from
434 HyMOD is evident (see for example Figure 6). However, differences in predictions from TVP-HBV and
435 TVP-HyMOD are more striking due to the lack of state updating. Figure 7 shows annual statistics of
436 simulated streamflow from the TVP-HBV and TVP-HyMOD models and observed runoff. The TVP-
437 HBV gives direct runoff and baseflow predictions that are consistent with runoff observations,
438 meaning that the parameter adjustments reflect the observed changes in the runoff response. This
439 however is not the case for the TVP-HyMOD. The annual runoff coefficient and annual direct runoff

coefficient are severely under-estimated in the post-change period by the TVP-HyMOD, whilst the Annual Baseflow Index has an increasing trend of magnitude far greater than observed (Figure 7c). All three quantities on the other hand are well represented by the TVP-HBV (Figure 7). Similar conclusions can be drawn from Figure 8, which shows the results of a Moving Average Shifting Horizon (MASH) analysis (see Section 2.2) on total and direct runoff (observed and simulated). Observed increases in January to April flows (see Figure 8a) and wet season direct flows (July to September) (see Figure 8e) are well represented by the TVP-HBV but not TVP-HyMOD.

The reason for the differences in performance between the TVP-HBV and TVP-HyMOD lies in the structure of the hydrologic model. The TVP-HyMOD is incapable of representing the observed increase in annual runoff/direct runoff coefficient due to the increased baseflow during dry periods, despite having an Annual Baseflow Index far greater than the observed. This occurs due to an inability to generate flow volume during periods of no rain. In joint state-parameter updating using HyMOD, underestimated runoff predictions during dry periods lead to adjustments to the k_s and α parameters to increase baseflow depth (since these are the only parameters that are associated to an active store). Unlike HBV, HyMOD has no continuous supply of water to the routing stores (i.e. the quick flow and slow flow stores) during recession periods (which typically have extended periods of no rainfall, so that V in Figure 3 is zero). This means that k_s and α are updated to extreme values to compensate for the volumetric shortfall. The HBV structure, on the other hand, has a continuous percolation of water into the deep layer store even during periods of no rain (so long as the shallow water store is non-empty). In summary, the HyMOD model structure is poorly suited to simulating streamflow dynamics in post-change conditions, although it gave reasonable simulations in pre-change conditions. This highlights that need to select a sufficiently flexible model structure prior to undertaking forecasting/predictive modelling using the time varying parameter approach. In particular, the model structure must be capable of effectively simulating all potential future catchment conditions.

Having established that the TVP-HBV provided a good representation of the observed streamflow dynamics, we used a modelling approach to determine whether the observed changes were solely driven by forcings and which (if any) components of runoff were also affected by land use change. A resampled rainfall and temperature time series was generated by sampling the data without replacement across years for each day (for instance rainfall and temperature for 1st January 1990 is found by randomly sampling from all records on 1st January). This maintains the intra-annual (e.g. seasonal) variability but destroys any inter-annual trends in the meteorological data. Streamflow simulations were then generated using this resampled meteorological sequence as inputs to the TVP-HBV (i.e. without state updating). If the resulting streamflow simulations do not reproduce the observed changes to streamflow dynamics, then this indicates that changes to meteorological forcings are the main contributor. However, if it is able to at least partially (or fully) reproduce the observed streamflow changes, this means that land cover changes are impacting catchment hydrology (but potentially in addition to forcing changes, due to the presence of ecosystem feedbacks). Figure 8d&h show the results of a MASH undertaken on the resulting simulations of total and direct runoff using the resampled forcing time series and TVP-HBV model. Observed increases in baseflow during the January – April period (see Figure 8a) and increases in direct runoff in the June – September period (see Figure 8e) are reproduced. The magnitude of increase in direct runoff in July is slightly lower, indicating the potential for some climatic influences also. This is consistent with findings from the Mann-Kendall test which identified a statistically significant increase in July rainfall (see Section 2.2). Overall however, these results lend further weight to the conclusion that land cover change has impacted the hydrologic regime of the Nammuc catchment. These results also demonstrate that parameter changes correspond to actual changes in catchment hydrology, and are not just random fluctuations that reproduce the observed streamflow statistics only when the observed forcing time series is used.

5. Conclusions

As our anthropogenic footprint expands, it will become increasingly important to develop modelling methodologies that are capable of handling changing catchment conditions. Previous work proposed the use of models whose parameters vary with time in response to signals of change in observations. The so-called Locally Linear Dual EnKF time varying parameter estimation algorithm [*Pathiraja et al.,* 2016a] was applied to 2 sets of small (< 350 ha) paired experimental catchments with deforestation occurring under experimental conditions (rapid clearing of 100% and 50% of land surface) [*Pathiraja et al.,* 2016b]. Here we demonstrate the efficacy of the method for a larger catchment experiencing more realistic land cover change, whilst also investigating the importance of the chosen model structure in ensuring the success of the time varying parameter estimation method. We also demonstrate that the time varying parameter framework can be used in a retrospective fashion to determine whether land cover changes (and not just meteorological factors) contribute to the observed hydrologic changes.

Experiments were undertaken on the Nammuc catchment (2880 km^2) in Vietnam, which experienced a relatively gradual conversion from forest to cropland over a number of years (cropland increased from roughly 23% of the catchment between 1981 and 1994 to 52% by 2000). Changes to the hydrologic regime after the mid-1990s were detected and attributed mostly to an increase in baseflow volume. Application of the LL Dual EnKF with two conceptual models (HBV and HyMOD) showed that the time varying parameter framework with state updating improved streamflow prediction in post-change conditions compared to the time invariant parameter case. However, baseflow predictions from the LL Dual EnKF with HBV were generally superior to the HyMOD case which tended to have a slight negative bias. It was found that the structure (i.e. model equations) of HyMOD was unsuited to representing the modified baseflow conditions, resulting in extreme and unrealistic time varying parameter estimates. This work shows that the chosen model is critical for

ensuring the time varying parameter framework successfully models streamflow in unknown future land cover conditions, particularly when used in a real time forecasting mode. Appropriate model selection can be a difficult task due to the significant uncertainty associated with future land use change, and can be even more problematic when multiple models have similar performance in pre-change conditions (as was the case in this study). One possible way to ensure success of the time varying parameter approach is to use models whose fundamental equations explicitly represent key physical processes (for instance, modelling sub-surface flow using Richard's equation with hydraulic conductivity allowed to vary with time). In this way, time variations in model parameters would more closely reflect changes to physiographic properties, rather than also having to account for missing processes. The drawback of such physically based models is that they are generally data intensive, both in generating model simulations (i.e. detailed inputs) and specifying parameters. Additionally, it may be necessary to reduce the dimensionality of the time varying parameter vector by keeping less sensitive model parameters fixed in order to make the estimation problem tractable. Models of intermediate complexity that have explicit process descriptions may be the most promising, although this also remains to be demonstrated.

6. Acknowledgements

This study was funded by the Australian Research Council as part of the Discovery Project DP140102394. Dr Marshall is additionally supported through a Future Fellowship FT120100269.

The data used in this paper were collected under the project IMRR (Integrated and sustainable water Management of Red Thai Binh Rivers System in changing climate), funded by the Italian Ministry of Foreign Affairs (Delibera n. 142 del 8 Novembre 2010). We greatly acknowledge Dr. Andrea Castelletti for provision of data and for discussions on this work.

Data utilized in this study can be made available from the authors upon request.

7. References

Aksoy, A., Zhang, F., Nielsen-Gammon, J. (2006). Ensemble-Based Simultaneous State and Parameter Estimation in a Two-Dimensional Sea-Breeze Model. *Monthly Weather Review*, 134, 2951–2970.

Alam, M., Islam, M., Salahin, N., and Hasanuzzaman, M. (2014) Effect of tillage practices on soil properties and crop productivity in wheat-mungbean-rice cropping system under subtropical climatic conditions. *The Scientific World Journal* 2014, https://www.hindawi.com/journals/tswj/2014/437283/

Anghileri, D., Pianosi, F., & Soncini-Sessa, R. (2014). Trend detection in seasonal data: From hydrology to water resources. *Journal of Hydrology*, *511*, 171–179. http://doi.org/10.1016/j.jhydrol.2014.01.022

Bergström, S. 1995. The HBV model. In: Singh, V.P. (Ed.) *Computer Models of Watershed Hydrology*. Water Resources Publications, Highlands Ranch, CO., pp. 443-476.

Bhaduri, B. B., Minner, M., Tatalovich, S., Member, A., & Harbor, J. (2001). Long-term hydrologic impact of urbanization: A tale of two models. *Journal of Water Resources Planning and Management*, *127*(February), 13–19.

Bormann, H., and K. Klaassen (2008) Seasonal and land use dependent variability of soil hydraulic and soil hydrological properties of two Northern German soils. *Geoderma* 145.3-4 (2008): 295-302. https://www.sciencedirect.com/science/article/pii/S0016706108000918#bib6

Boyle, D. (2001). Multicriteria calibration of hydrological models, *Ph.D. dissertation*, Univ. of Ariz., Tucson.

Brown, A. E., Mcmahon, T. A., Podger, G. M., & Zhang, L. (2006). A methodology to predict the impact of changes in forest cover on flow duration curves, *CSIRO Land and Water Science Report 8/06*.

Brown, A. E., Western, A. W., McMahon, T. a., & Zhang, L. (2013). Impact of forest cover changes on annual streamflow and flow duration curves. *Journal of Hydrology*, *483*, 39–50. http://doi.org/10.1016/j.jhydrol.2012.12.031

Clark, M. P., Rupp, D. E., Woods, R. A., Zheng, X., Ibbitt, R. P., Slater, A. G., … Uddstrom, M. J. (2008). Hydrological data assimilation with the ensemble Kalman filter: Use of streamflow observations to update states in a distributed hydrological model. *Advances in Water Resources*, *31*(10), 1309–1324. http://doi.org/10.1016/j.advwatres.2008.06.005

Coe, M. T., Latrubesse, E. M., Ferreira, M. E., & Amsler, M. L. (2011). The effects of deforestation and climate variability on the streamflow of the Araguaia River, Brazil. *Biogeochemistry*, *105*(1–3), 119–131. http://doi.org/10.1007/s10533-011-9582-2

Coron, L., Andréassian, V., Perrin, C., Lerat, J., Vaze, J., Bourqui, M., & Hendrickx, F. (2012). Crash testing hydrological models in contrasted climate conditions: An experiment on 216 Australian catchments. *Water Resources Research,* 48(5), 1–17. http://doi.org/10.1029/2011WR011721

577 Costa, M. H., Botta, A., & Cardille, J. A. (2003). Effects of large-scale changes in land cover on the
578 discharge of the Tocantins River, Southeastern Amazonia. *Journal of Hydrology*, *283*(1–4), 206–
579 217. http://doi.org/10.1016/S0022-1694(03)00267-1

580 Duan, Q. Y., Gupta, V. K., & Sorooshian, S. (1993). Shuffled complex evolution approach for effective
581 and efficient global minimization. *Journal of Optimization Theory and Applications*, *76*(3), 501–
582 521. http://doi.org/10.1007/BF00939380

583 Dwarakish, G. S., & Ganasri, B. P. (2015). Impact of land use change on hydrological systems: A
584 review of current modeling approaches. *Cogent Geoscience*, *1*(1), 1115691–1115691.
585 http://doi.org/10.1080/23312041.2015.1115691

586 Eckhardt, K. (2005). How to construct recursive digital filters for baseflow separation. *Hydrological*
587 *Processes*, *19*(2), 507–515. http://doi.org/10.1002/hyp.5675

588 Efstratiadis, A., Nalbantis, I., & Koutsoyiannis, D. (2015). Hydrological modelling of temporally-varying
589 catchments: facets of change and the value of information. *Hydrological Sciences Journal*, *60*(7–
590 8), 1438–1461. http://doi.org/10.1080/02626667.2014.982123

591 Elfert, S., & Bormann, H. (2010). Simulated impact of past and possible future land use changes on
592 the hydrological response of the Northern German lowland "Hunte" catchment. *Journal of*
593 *Hydrology*, 383, 245–255. http://dx.doi.org/10.1016/j.jhydrol.2009.12.040

594 Evensen, G. (1994). Sequential data assimilation with a nonlinear quasi-geostrophic model using
595 Monte Carlo methods to forecast error statistics. *Journal of Geophysical Research*, *99*(C5).
596 http://doi.org/10.1029/94JC00572

597 FAO (2005). Global Forest Resources Assessment 2005 (FRA 2005)

598 Good, I.J. (1952). Rational Decisions. *Journal of the Royal Statistical Society.* B 14: 107–114.
599
600 Gu, Y., and D. S. Oliver (2005), History matching of the PUNQ-S3 reservoir model using the ensemble
601 Kalman filter, *SPE J.*, *10*(2), 217–224, http://doi.org/10.2118/89942-PA.
602
603 Giuliani, M., Anghileri, D., Castelletti, A., Vu, P. N., & Soncini-Sessa, R. (2016). Large storage
604 operations under climate change: expanding uncertainties and evolving tradeoffs.
605 *Environmental Research Letters*, 11(3), 035009.
606
607 Hadka, D., Reed, P., (2013). Borg: an auto–adaptive many–objective evolutionary computing
608 framework. *Evol. Comput*. 21 (2), 231–259.

609 Hamon, W. (1961). Estimating potential evapotranspiration. *Transactions of the American Society of*
610 *Civil Engineers*, 128(1), pp.324-337.

611 Kalman, R.E. (1960) A new approach to linear filtering and prediction problems, Transactions of the
612 ASME – *Journal of Basic Engineering*, Series D, 82 (1960), 35–45.

613 Kavetski, D., Kuczera, G., & Franks, S. W. (2006). Bayesian analysis of input uncertainty in hydrological
614 modeling: 1. Theory. *Water Resources Research*, *42*(3), http://doi.org/10.1029/2005WR004368
615

Keppeler, E. T., and R. R. Ziemer (1990) Logging effects on streamflow: water yield and summer low flows at Caspar Creek in northwestern California. *Water Resources Research* 26.7 (1990): 1669-1679.
http://onlinelibrary.wiley.com/doi/10.1029/WR026i007p01669/full

Kim, D.-H., J. O. Sexton, and J. R. Townshend (2015). Accelerated deforestation in the humid tropics from the 1990s to the 2000s, *Geophysical Research Letters*, 42, 3495–3501, http://doi.org/10.1002/ 2014GL062777.

Komma, J., G. Blöschl, and C. Reszler (2008), Soil moisture updating by Ensemble Kalman Filtering in real-time flood forecasting, *J. Hydrol.*, *357*(3–4), 228–242, http://doi.org/10.1016/j.jhydrol.2008.05.020.

Kummer, D., and Turner, B. (1994). The Human Causes of Deforestation in Southeast Asia. *BioScience, 44*(5), 323-328. http://doi.org/10.2307/1312382

Legesse, D., Vallet-Coulomb, C., & Gasse, F. (2003). Hydrological response of a catchment to climate and land-use changes in Tropical Africa: case study South Central Ethiopia. *Journal of Hydrology*, *275*(1-2), 67–85. http://doi.org/10.1016/S0022-1694(03)00019-2

Marshall, L., Sharma, A. and Nott, D. (2006) 'Modeling the catchment via mixtures: Issues of model specification and validation', *Water Resources Research*, 42(11), pp. 1–14. http://doi.org/ 10.1029/2005WR004613.

McIntyre, N., & Marshall, M. (2010). Identification of rural land management signals in runoff response. *Hydrological Processes*, *24*(24), 3521–3534. http://doi.org/10.1002/hyp.7774

McMillan, H., Jackson, B., Clark, M., Kavetski, D., & Woods, R. (2011). Rainfall uncertainty in hydrological modelling: An evaluation of multiplicative error models. *Journal of Hydrology*, *400*(1-2), 83–94. http://doi.org/10.1016/j.jhydrol.2011.01.026

Moradkhani, H., Sorooshian, S., Gupta, H. V., & Houser, P. R. (2005). Dual state–parameter estimation of hydrological models using ensemble Kalman filter. *Advances in Water Resources*, *28*(2), 135–147. http://doi.org/10.1016/j.advwatres.2004.09.002

Niu, J., & Sivakumar, B. (2013). Study of runoff response to land use change in the East River basin in South China. *Stochastic Environmental Research and Risk Assessment*. http://doi.org/10.1007/s00477-013-0690-5

Nossent, J., P. Elsen, and W. Bauwens. (2011) Sobol'sensitivity analysis of a complex environmental model. *Environmental Modelling & Software* 26.12 (2011): 1515-1525.

Pathiraja, S., Marshall, L., Sharma, A., & Moradkhani, H. (2016a). Hydrologic modeling in dynamic catchments: A data assimilation approach. *Water Resources Research*, *52*, 3350–3372. http://doi.org/10.1002/2015WR017192

Pathiraja, S., Marshall, L., Sharma, a., & Moradkhani, H. (2016b). Detecting non-stationary hydrologic model parameters in a paired catchment system using data assimilation. *Advances in Water Resources*, *94*, 103–119. http://doi.org/10.1016/j.advwatres.2016.04.021

Pianosi, F., Sarrazin, F., Wagener, T. A Matlab toolbox for Global Sensitivity Analysis, *Environmental*

661 *Modelling & Software*, 70, 80-85, http://dx.doi.org/10.1016/j.envsoft.2015.04.009.

662 Price, K. (2011). Effects of watershed topography, soils, land use, and climate on baseflow hydrology
663 in humid regions: A review. *Progress in physical geography* 35.4 (2011): 465-492.
664 http://journals.sagepub.com/doi/abs/10.1177/0309133311402714#articleCitationDownloadCon
665 tainer

666 Reed, P. M., Hadka, D., Herman, J. D., Kasprzyk, J. R., & Kollat, J. B. (2013). Evolutionary
667 multiobjective optimization in water resources: The past, present, and future. *Advances in water*
668 *resources*, *51*, 438-456.

669 Reichle, R. H., D. B. McLaughlin, and D. Entekhabi (2002), Hydrologic Data Assimilation with the
670 Ensemble Kalman Filter, *Am. Meteorol. Soc. - Mon. Weather Rev.*, *130*(1), 103–114,
671 http://doi.org/10.1175/1520-0493(2002)130<0103:HDAWTE>2.0.CO;2.

672 Rose, S., & Peters, N. E. (2001). Effects of urbanization on streamflow in the Atlanta area (Georgia,
673 USA): a comparative hydrological approach. *Hydrological Processes*, *15*(8), 1441–1457.
674 http://doi.org/10.1002/hyp.218

675 Saltelli, A., Ratto, M., Andres, T., Campolongo, F., Cariboni, J., Gatelli, D., Saisana, M., Tarantola, S.,
676 (2008). Global Sensitivity Analysis, the Primer. Wiley.

677 Seibert, J., & McDonnell, J. J. (2010). Land-cover impacts on streamflow: a change-detection
678 modelling approach that incorporates parameter uncertainty. *Hydrological Sciences Journal*,
679 *55*(3), 316–332. http://doi.org/10.1080/02626661003683264
680
681 Sun, A. Y., A. Morris, and S. Mohanty (2009), Comparison of deterministic ensemble Kalman filters for
682 assimilating hydrogeological data, *Adv. Water Resour.*, *32*(2), 280–292,
683 http://doi.org/10.1016/j.advwatres.2008.11.006.

684 Taver, V., Johannet, a., Borrell-Estupina, V., & Pistre, S. (2015). Feed-forward vs recurrent neural
685 network models for non-stationarity modelling using data assimilation and adaptivity.
686 *Hydrological Sciences Journal*, *60*(7–8), 1242–1265.
687 http://doi.org/10.1080/02626667.2014.967696

688 Thanapakpawin, P., Richey, J., Thomas, D., Rodda, S., Campbell, B., & Logsdon, M. (2007). Effects of
689 landuse change on the hydrologic regime of the Mae Chaem river basin, NW Thailand. *Journal*
690 *of Hydrology*, *334*(1-2), 215–230. http://doi.org/10.1016/j.jhydrol.2006.10.012
691
692 Villarini, G., & Krajewski, W. F. (2008). Empirically-based modeling of spatial sampling uncertainties
693 associated with rainfall measurements by rain gauges. *Advances in Water Resources*, *31*(7),
694 1015–1023. http://doi.org/10.1016/j.advwatres.2008.04.007
695
696 Vu, V.T., 1993. Evaluation of the impact of deforestation to inflow regime of the Hoa Binh Reservoir
697 in Vietnam, Hydrology of Warm Humid Regions (Proceedings of the Yokohama Symposium,
698 July 1993). IAHS Publ. no. 216
699
700 Wang, J., Ishidaira, H., & Xu, Z. X. (2012). Effects of climate change and human activities on inflow
701 into the Hoabinh Reservoir in the Red River basin. *Procedia Environmental Sciences*, *13*, 1688-
702 1698.

703 Warburton, M. L., Schulze, R. E., & Jewitt, G. P. W. (2012). Hydrological impacts of land use change in
704 three diverse South African catchments. *Journal of Hydrology*, *414–415*, 118–135.
705 http://doi.org/10.1016/j.jhydrol.2011.10.028

706 Weerts, A. H., & El Serafy, G. Y. H. (2006). Particle filtering and ensemble Kalman filtering for state
707 updating with hydrological conceptual rainfall-runoff models. *Water Resources Research*, *42*(9),
708 n/a-n/a. http://doi.org/10.1029/2005WR004093

709 Westra, S.; Thyer, M.; Leonard, M.; Kavetski, D.; Lambert, M. (2014). A strategy for diagnosing and
710 interpreting hydrological model nonstationarity. *Water Resources Research*, 5090–5113.
711 http://doi.org/10.1002/2013WR014719.Received

712 Wijesekara, G. N., Gupta, A., Valeo, C., Hasbani, J. G., Qiao, Y., Delaney, P., & Marceau, D. J. (2012).
713 Assessing the impact of future land-use changes on hydrological processes in the Elbow River
714 watershed in southern Alberta, Canada. *Journal of Hydrology*, *412–413*, 220–232.
715 http://doi.org/10.1016/j.jhydrol.2011.04.018

716 WWF. (2013). Ecosystems in the Greater Mekong: Past trends, current status, possible futures.

717 Xie, X., Meng, S., Liang, S., & Yao, Y. (2014). Improving streamflow predictions at ungauged locations
718 with real-time updating: application of an EnKF-based state-parameter estimation strategy.
719 *Hydrology and Earth System Sciences*, *18*(10), 3923–3936. http://doi.org/10.5194/hess-18-
720 3923-2014

721 Xu, T., and J. . Gomez-Hernandez (2016), Joint identification of contaminant source location, initial
722 release time, and initial solute concentration in an aquifer via ensemble kalman filtering, *Water*
723 *Resour. Res.*, 600–612, http://doi.org/10.1002/2015WR018249.

724 Yang, L., Wei, W., Chen, L., & Mo, B. (2012). Response of deep soil moisture to land use and
725 afforestation in the semi-arid Loess Plateau, China. *Journal of Hydrology*, *475*, 111–122.
726 http://doi.org/10.1016/j.jhydrol.2012.09.041

727 Zimmermann, B., H. Elsenbeer, and J. M. De Moraes. (2006) The influence of land-use changes on soil
728 hydraulic properties: implications for runoff generation. *Forest ecology and management* 222.1-
729 3 (2006): 29-38.

730 # Tables

	Pre 1994	Post 1994
Land Use		
Evergreen Forest (including evergreen needle and evergreen leaf) (%)	77%	48%
Cropland (%)	23%	52%
Hydro-Meteorological Properties		
Mean Annual Rainfall (mm)	1630	1660
Mean Annual Runoff (mm)	838	1190
Mean Annual Runoff Coefficient	0.5	0.7
Mean Annual PET (mm)	1300	1300
Estimated Mean Annual BFI	0.33	0.39

731 **Table 1 Study catchment properties**

732

733

734

735

736

737

738

	HYMOD	HBV
NSE [ ]	**0.77**	0.75
Peak flows (q > 5mm/d)		
MAE [mm/d]	3.11	**2.85**
RMSE [mm/d]	**4.55**	4.72
Medium flows (1 mm/d <= q <= 5mm/d)		
MAE [mm/d]	**0.66**	0.80
RMSE [mm/d]	**0.86**	1.09
Low flows (q < 1mm/d)		
MAE [mm/d]	0.35	**0.20**
RMSE [mm/d]	0.42	**0.34**

739 **Table 2 Model performance in pre-change conditions used for calibration (1975 – 1979). Bold face**
740 **numbers correspond to the model with superior performance for the particular metric.**

741

742

743

744

	Sensitivity Index
hl1	0.10
lp	0.12
Maxbas	0.14
fcap	0.18
K0	0.23
K2	0.23
K1	0.38
beta	0.41
perc	0.47

745 **Table 3 Variance Based Sensitivity Analysis Results for HBV parameters: first order sensitivity index**
746 **representing the contribution of varying a single parameter to the variance of the model output.**
747 **Lower values indicate lower sensitivity.**

748

749

750

751

752

Parameters						
	Description	**Units**	**Initial Sampling Distribution**	**Feasible Range**	s^2	**Max allowable daily rate of change (m_{max})**
β	Soil Moisture exponent	[ ]	*N*(2, 0.1)	0 – 7	0.003	1.8×10^{-3}
$fcap$	Maximum soil moisture store depth	[mm]	*N*(467, 10)	10 – 2000	0.003	0.4
$hl1$	Threshold for generation of near surface flow	[mm]	*N*(120, 10)	0 – 400	0.003	0.1
$K0$	Near Surface Flow Routing Coefficient	[ ]	*N*(0.3, 0.005)	0.0625 – 1	0.003	2×10^{-4}
$K1$	Interflow Routing Coefficient	[ ]	*N*(0.09, 5×10^{-4})	0.02 – 0.1	0.003	9×10^{-6}
$perc$	Percolation rate	[mm/d]	*N*(1.3, 10^{-4})	0 – 3	0.003	10^{-3}
$K2$	Baseflow Routing Coefficient	[ ]	*N*(0.01, 10^{-6})	5×10^{-5}– 0.02	0.003	9×10^{-6}
States						
$sowat$	Soil Moisture Store	[mm]	*N*(0,1)	(0, $fcap$)		
$stw1$	Shallow Layer Store	[mm]	*N*(0,1)	(0, ∞)		
$stw2$	Deep Layer Store	[mm]	*N*(0,0.1)	(0, ∞)		

753 **Table 4 Locally Linear EnKF inputs for the HBV model case**

754

755

Parameters						
	Description	**Units**	**Initial Sampling Distribution**	**Feasible Range**	s^2	**Max allowable daily rate of change (m_{max})**
b	Pareto-distributed soil storage shape parameter	[ ]	$N(0.37, 10^{-4})$	0 – 0.3	0.004	$3x10^{-4}$
c_{max}	Maximum point soil storage depth	[mm]	$N(651, 10)$	300 – 1500	0.004	0.3
k_q	Quick flow Routing Coefficient	[ ]	$N(0.6, 5x10^{-4})$	0.55 – 0.99	0.018	$3x10^{-4}$
k_s	Slow flow Routing Coefficient	[ ]	$N(0.04, 5x10^{-4})$	0.001 – 0.54	0.018	$4x10^{-5}$
α	Excess Runoff Splitting Parameter	[ ]	$N(0.47, 5x10^{-4})$	0.001 – 0.99	0.018	$4x10^{-4}$
States						
S	Soil Store	[mm]	$N(180, 0.1*180)$	$(0, S_{max} = \frac{bc_{min}+c_{max}}{b+1})$		
$S_{q1,2,3}$	Quick Flow Stores	[mm]	$N(0,1)$	$(0, \infty)$		
S_s	Slow Flow Store	[mm]	$N(0,1)$	$(0, \infty)$		

Table 5 Locally Linear EnKF inputs for the HYMOD model case

Figures

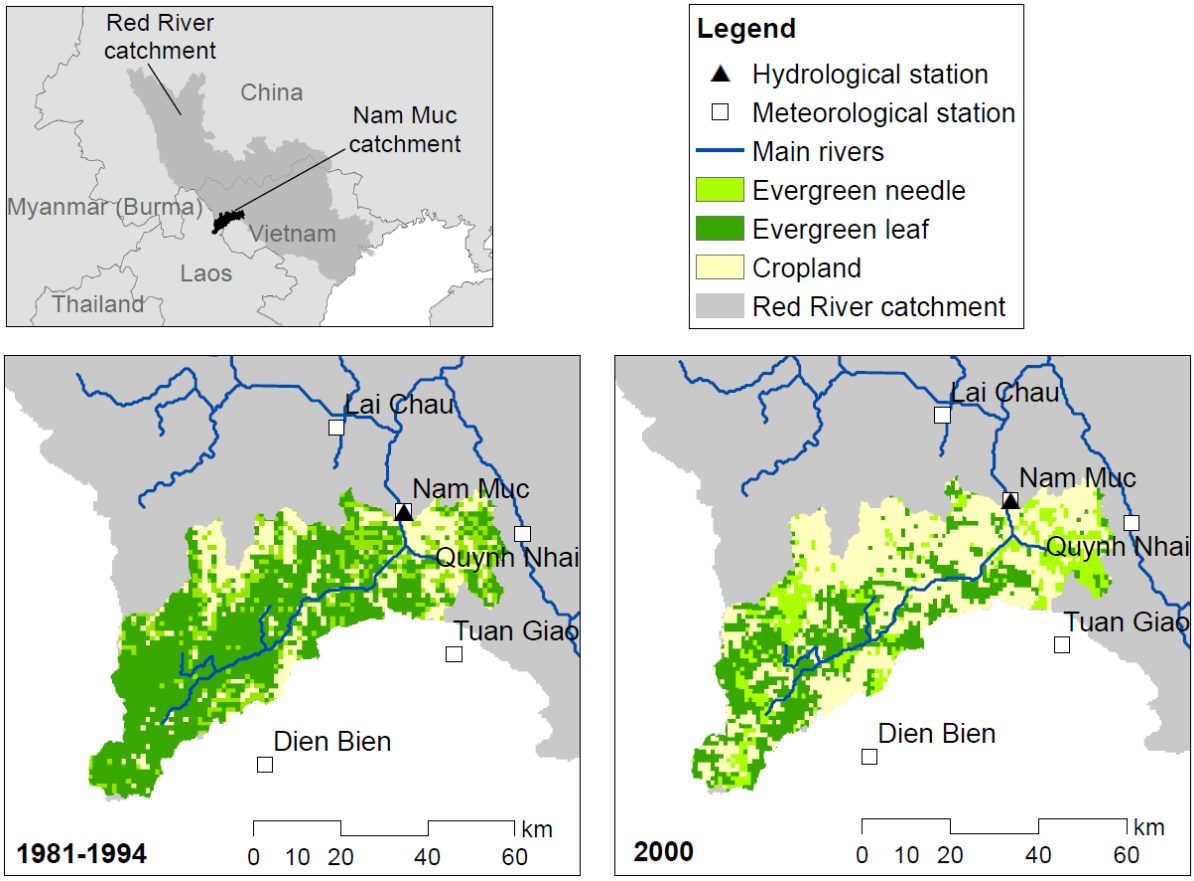

Figure 1 Study Catchment showing gauges and changes in land cover over time.

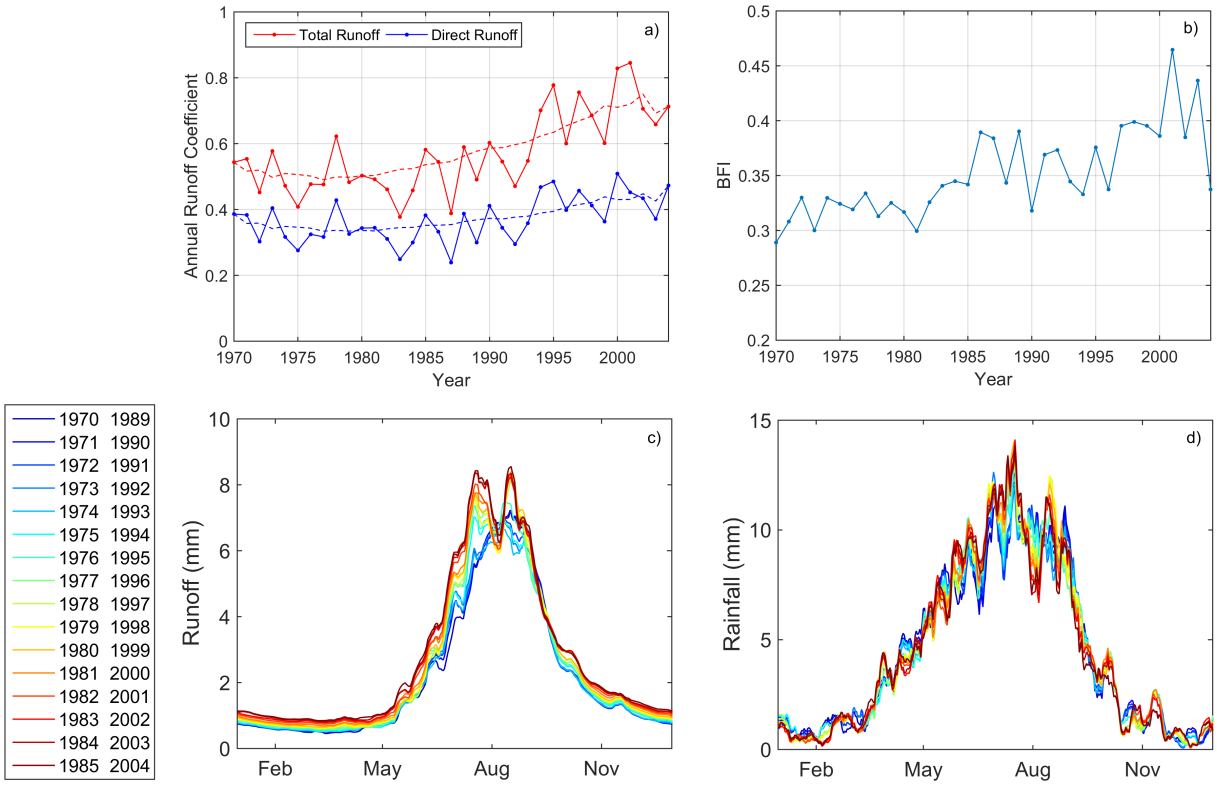

Figure 2 Impact of land use change on observed streamflow: a) Annual Runoff Coefficient, b) Annual Baseflow Index (BFI), c) Moving Average Shifting Horizon (MASH) results for total observed runoff, d) MASH for observed rainfall.

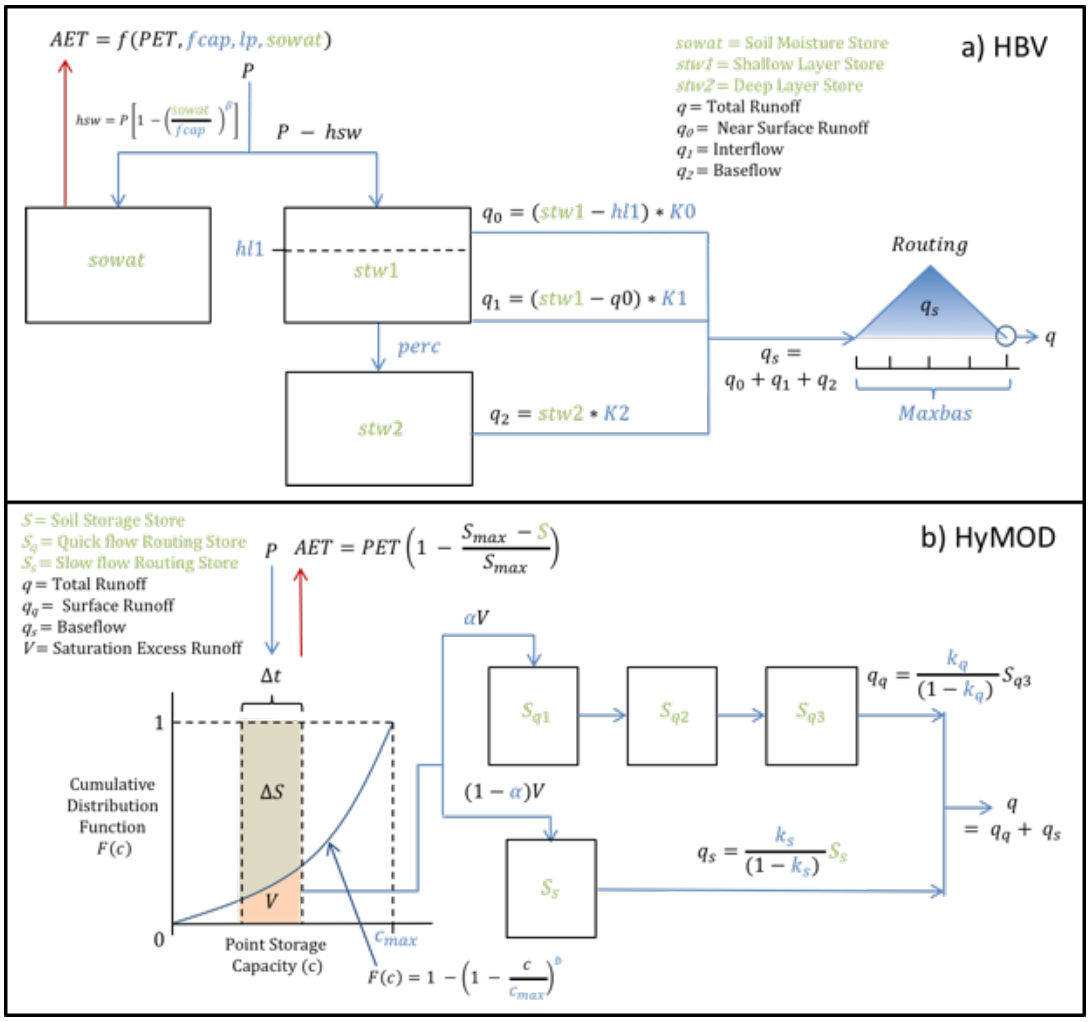

794

795 **Figure 3 Schematic of the models used in this study: a) HBV and b) HyMOD. Parameters are shown**
796 **in blue and states are shown in green.**

797

798

799

800

801

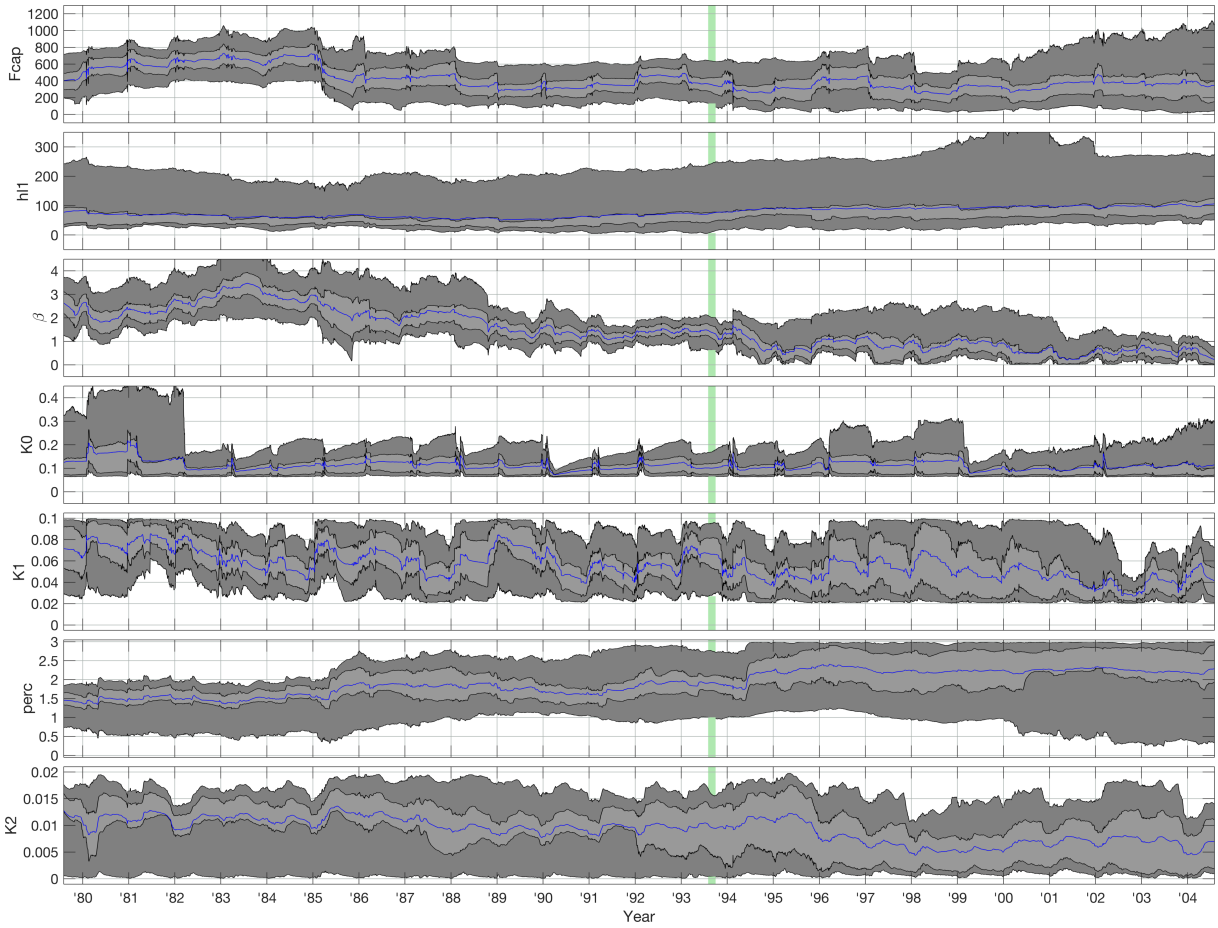

Figure 4 Parameter Trajectories using the HBV model. The dark grey shaded areas indicate the middle 90% of the ensemble, bounded by the 5th and 95th percentiles. The light grey shaded areas indicate the middle 50% of the ensemble, bounded by the 25th and 75th percentiles. The ensemble mean is indicated by the blue line. The vertical green panel indicates the assumed time period of rapid deforestation.

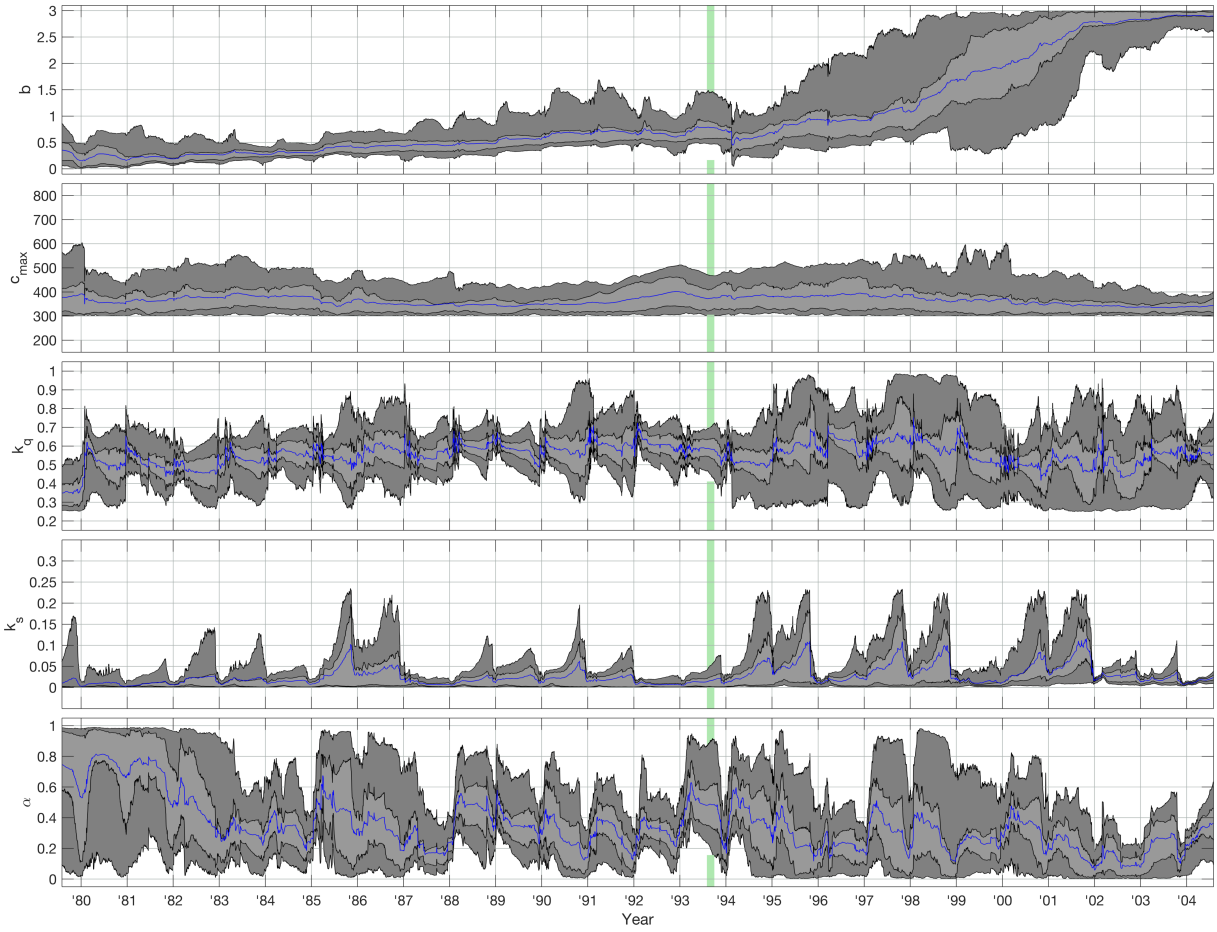

Figure 5 Parameter Trajectories using the HyMOD model. The dark grey shaded areas indicate the middle 90% of the ensemble, bounded by the 5th and 95th percentiles. The light grey shaded areas indicate the middle 50% of the ensemble, bounded by the 25th and 75th percentiles. The ensemble mean is indicated by the blue line. The vertical green panel indicates the assumed time period of rapid deforestation.

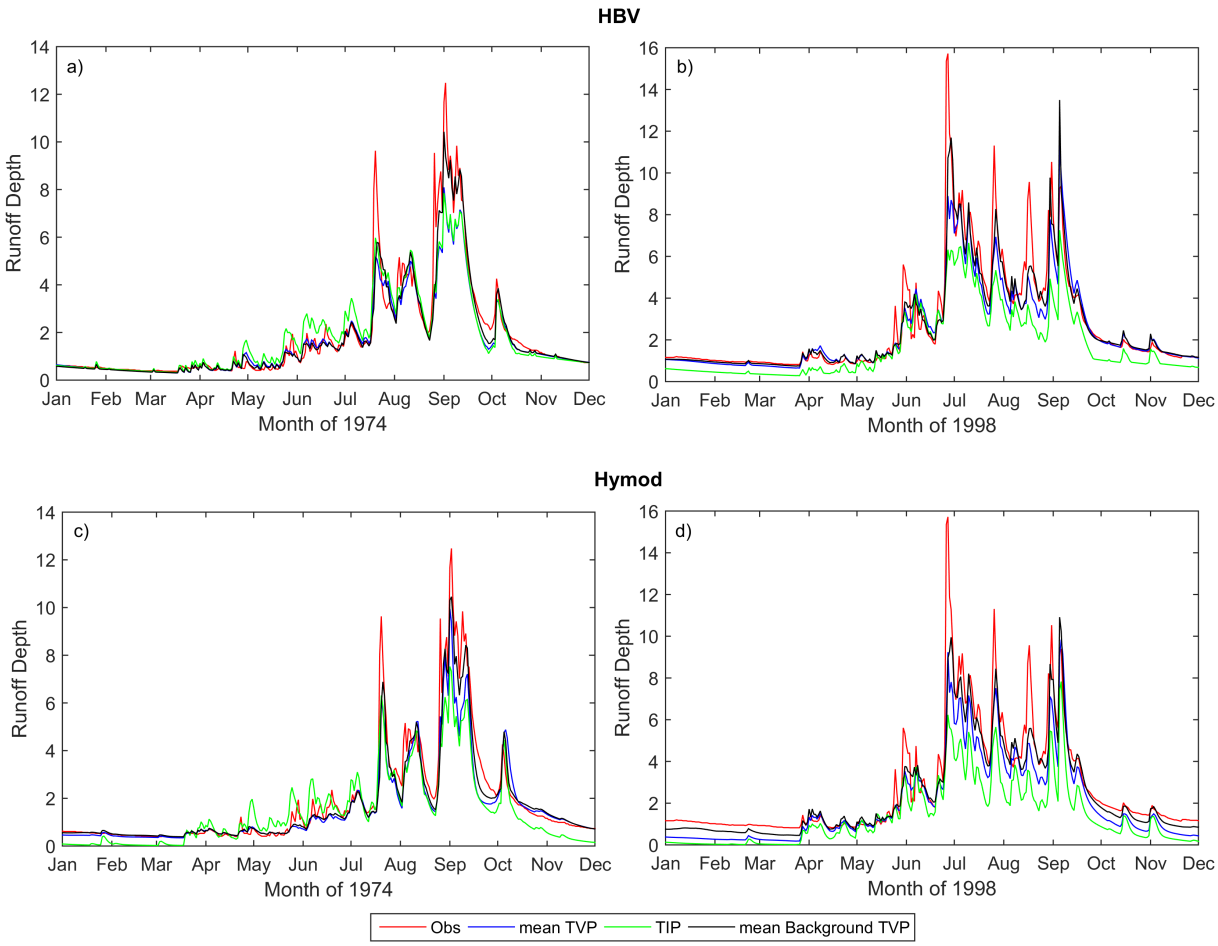

Figure 6 Representative Hydrographs of background streamflow from the LL Dual EnKF (black line), Time varying parameter model with no state updating (blue line), time invariant parameter model with no DA (green line) and observed streamflow (red line). Results for HBV are shown in the top row and HyMOD in the bottom row. A pre-change year (1974) is shown on the left and a post change year (1998) on the right.

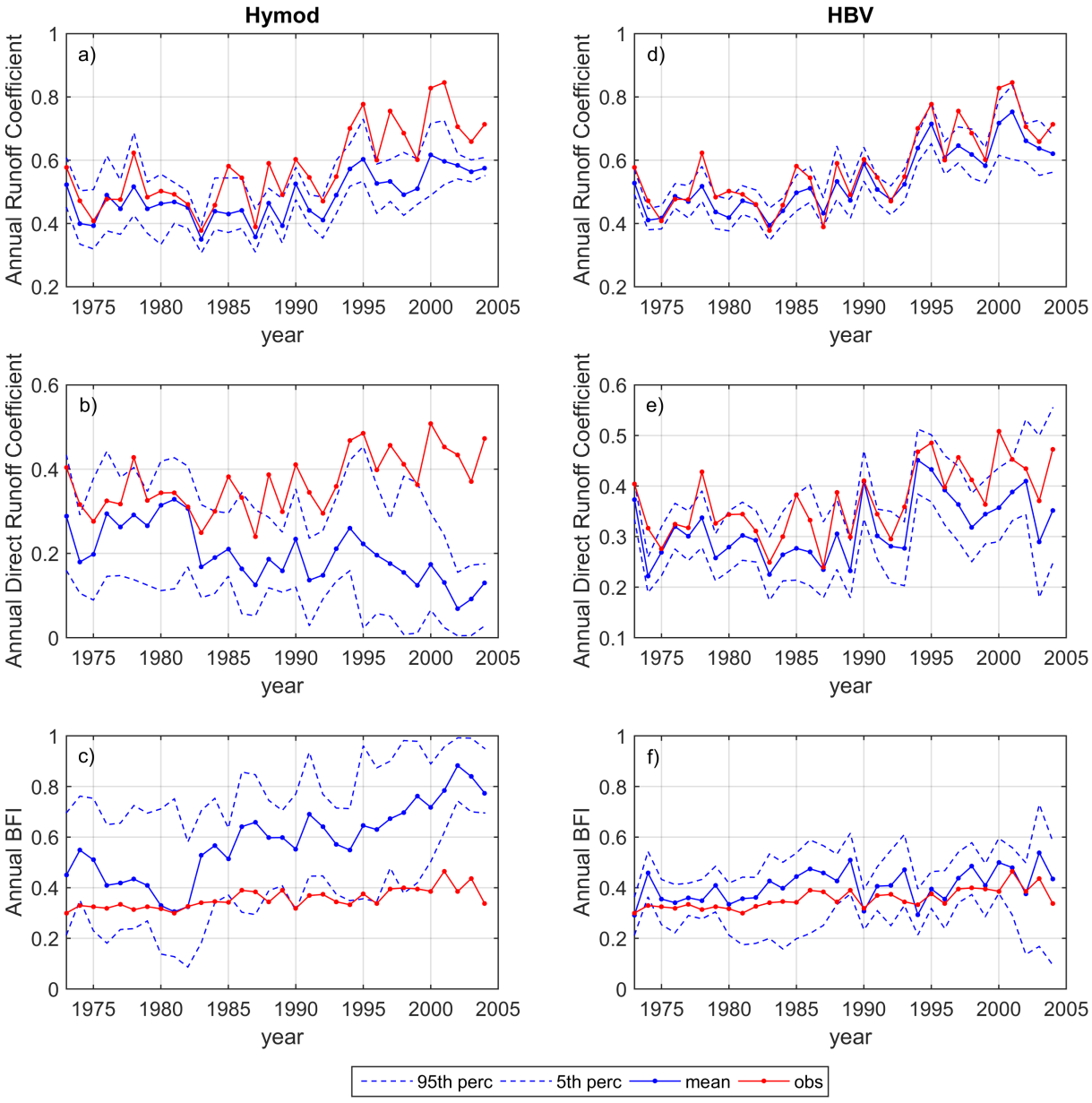

Figure 7 Influence of time varying parameters on model output (i.e. without state updating) summarized in terms of the Annual Runoff Coefficient (top row), Annual Direct Runoff Coefficient (second row) and Annual Baseflow Index (BFI) (third row). Results for HyMOD are shown in the first column, HBV are shown in the second column.

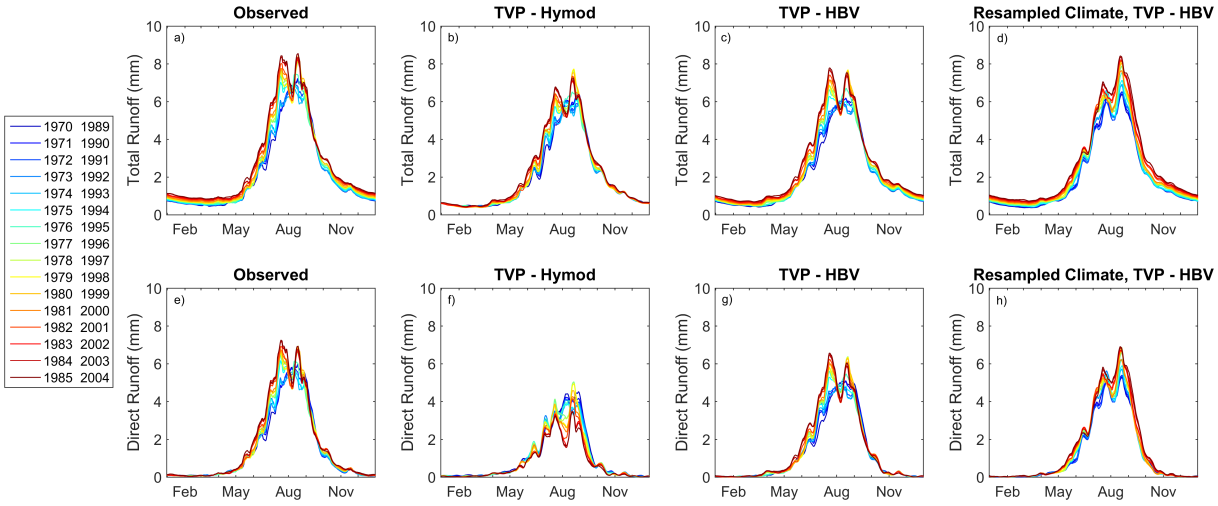

Figure 8 Moving Average Shifting Horizon (MASH) results for observed streamflow (first column), simulated streamflow from time varying parameter model (without state DA) for HYMOD (2nd column), HBV (third column), resampled climate HBV (fourth column). These are split into total runoff (first row) and direct runoff or surface runoff (2nd row).